Check for updates

Received: 26 October 2022 | Revised: 3 February 2023 | Accepted: 13 February 2023

DOI: 10.1002/pro6.1189

ORIGINAL ARTICLE

WILEY

Evaluating bone marrow dosimetry with the addition of bone marrow structures to the medical internal radiation dose phantom

Kristine L. Ferrone[1,2,3] | Charles E. Willis[1,2] | Fada Guan[1,4] | Jingfei Ma[1,2] | Leif E. Peterson[5] | Stephen F. Kry[1,2]

[1]The University of Texas M.D. Anderson Cancer Center, Houston, Texas, USA

[2]The University of Texas M.D. Anderson Cancer Center UT Health Graduate School of Biomedical Sciences, Houston, Texas, USA

[3]The Aerospace Corporation, Houston, Texas, USA

[4]Department of Therapeutic Radiology, Yale University School of Medicine, New Haven, Connecticut, USA

[5]Department of Statistics, Rice University, Houston, Texas, USA

Correspondence
Kristine L. Ferrone
Email: kristine.ferrone@aero.org

[Correction added on 27th March 2023, after first online publication: The Fourth author name was updated.]

Funding information
The Aerospace Corporation, El Segundo, California.

Abstract

Background: Reliable estimates of radiation dose to bone marrow are critical to understanding the risk of radiation-induced cancers. Although the medical internal radiation dose phantom is routinely used for dose estimation, bone marrow is not defined in the phantom. Consequently, methods of indirectly estimating bone marrow dose have been implemented based on dose to surrogate volumes or average dose to soft tissue.

Methods: In this study, new bone marrow structures were implemented and evaluated to the medical internal radiation dose phantom in Geant4, offering improved fidelity. The dose equivalent to the bone marrow was calculated across medical, occupational, and space radiation exposure scenarios, and compared with results using prior indirect estimation methods.

Conclusion: Our results show that bone marrow dose may be overestimated by up to a factor of three when using the traditional methods when compared with the improved fidelity medical internal radiation dose method, specifically at clinical x-ray energies.

KEYWORDS
computational phantoms, Monte Carlo simulations, radiation dosimetry

1 | INTRODUCTION

Active bone marrow is a particularly radiosensitive structure in the human body, as evidenced by high rates of radiation-induced leukemia in atomic bomb survivors, workers in nuclear power and the nuclear weapons complex, medical workers, nuclear accident victims, and environmentally exposed members of the public.[1–4] Assessing the dose to bone marrow is important for medical, occupational, and space-related radiation exposures.

Organ doses from radiation exposures are routinely estimated using the medical internal radiation dose (MIRD) computational phantom. The MIRD phantom was first introduced in the 1970s as a tool for estimating the dose from internal radiation sources in nuclear medicine. In the decades since its introduction, applications of the MIRD phantom have grown substantially to include scenarios involving external medical, occupational, and space-related exposures.

However, bone marrow is not defined in the MIRD phantom, and early MIRD literature notes the lack of bone marrow volumes as a known limitation of the model.[5–7] Consequently, methods for indirectly estimating the dose to the bone marrow have been developed over the past several decades. Prior methods for calculating dose to active bone marrow in simulations using the MIRD phantom are to estimate the dose based on surrogate volumes or to use the average dose to the soft tissue.[5–13] There are limitations of each of these

This is an open access article under the terms of the Creative Commons Attribution-NonCommercial-NoDerivs License, which permits use and distribution in any medium, provided the original work is properly cited, the use is non-commercial and no modifications or adaptations are made.
© 2023 The Authors. *Precision Radiation Oncology* published by John Wiley & Sons Australia, Ltd on behalf of Shandong Cancer Hospital & Institute.

methods, including the inability to calculate the dose to a specific bone marrow volume, and dose inaccuracies for certain energy ranges and radiation species. Newer models have solved some of these issues for specific applications, primarily within the nuclear medicine community and involving internal radiation sources,[8–11,13] but these models vary in complexity and general applicability.

The present article describes a novel method for improving the fidelity of the traditional MIRD phantom by adding bone marrow volumes to the geometry. This improved fidelity MIRD phantom provides a more accurate representation of the human body that improves dose estimates and, therefore, can provide higher confidence in bone marrow dosimetry across many applications.

2 | METHODS

For the persent study, we conducted Monte Carlo simulations in Geant4[14] using the QBBC physics list and 10^9 initiated source particles per run. The geometry of the MIRD phantom was based on an example packaged with the GEANT4 version 10.03.p03 release (/examples/advanced/human_phantom). This geometry includes approximations of a 70-kg man and woman. In these approximations of the human body, not every organ structure is modeled; some structures, such as the bone marrow, are not defined, whereas other structures, such as specific bones, are approximated. Therefore, the MIRD phantom is termed a stylized computational phantom.[5–7]

The distribution of active bone marrow in an average 40-year-old adult was taken from the literature[15]. Approximations of the active bone marrow distribution based on the bone volumes present in the MIRD phantom were calculated; for example, the MIRD phantom does not include a mandible, so we increased the distribution of marrow in the cranium to account for the additional amount. Similarly, the bone marrow in the sternum, which is not defined in the MIRD phantom, was added to the rib contribution. Finally, the spine is divided into fewer sections in the MIRD phantom than in full human anatomy. A summary of the modifications to the bone marrow distribution for the bones present in the MIRD phantom, as compared with the bone marrow distribution from the literature, are given in Table 1.

The total mass of bone marrow in adults is approximately 4% of the total body mass,[16] with approximately half of this marrow being hematopoietic/red (active) marrow. Therefore, for the present 70-kg MIRD phantom, we set the total bone marrow mass to 3 kg and active marrow mass to 1.5 kg. We used a density of active bone marrow of 1.06 g/cm^3, with elemental composition described in the literature.[8]

To model the active bone marrow within the MIRD phantom in our simulations, we created daughter volumes for bone marrow within the bone volumes included in our MIRD phantom. To size the bone marrow daughter volume for each bone in the phantom, we performed calculations based on the active bone marrow distribution, average total bone marrow mass in adults, bone marrow density and composition, and the size and shape of each bone volume. Full details of these calculations are included in Appendix 1. Figure 1 shows a cutaway view of our

TABLE 1 Active bone marrow distribution for a 40-year-old adult from the literature[15] and medical internal radiation dose phantom modified in the present study.

Bone	% Active marrow (Cristy 1981)	% Active marrow (modified MIRD)
Cranium	7.6	8.4
Mandible	0.8	–
Scapulae	2.8	2.8
Clavicles	0.8	0.8
Ribs	16.1	19.2
Sternum	3.1	–
Upper spine	3.9	3.9
Mid-lower spine	–	38.4
Thoracic vertebrae	16.1	–
Lumbar vertebrae	12.3	–
Sacrum	9.9	–
Pelvis	17.5	17.5
Femora	6.7	6.7
Humeri	2.3	2.3

MIRD, medical internal radiation dose.

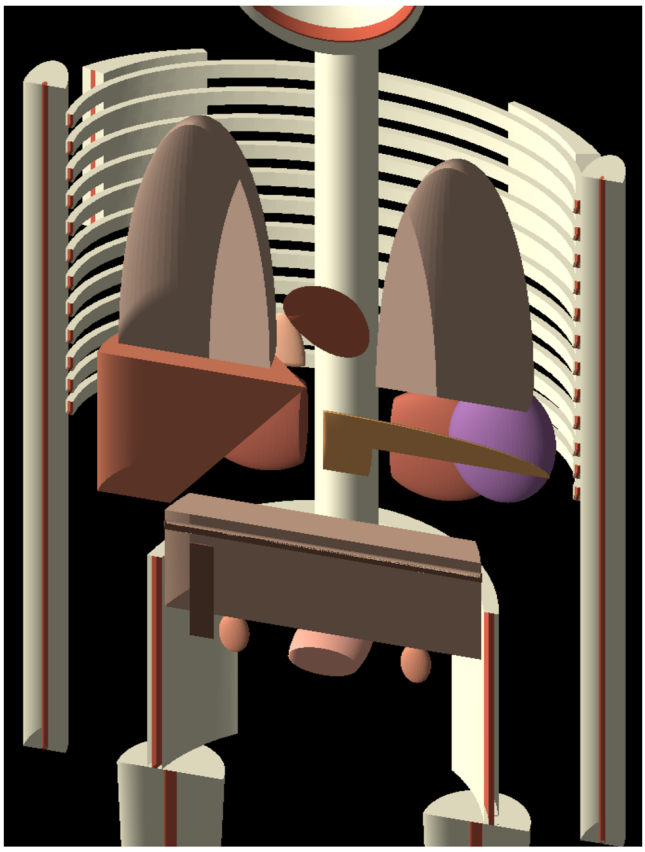

FIGURE 1 Modified medical internal radiation dose phantom modeled in Geant4 with active bone marrow volumes added in red.

23987324, 2023, 1, Downloaded from https://onlinelibrary.wiley.com/doi/10.1002/pro6.1189 by Rice University, Wiley Online Library on [24/04/2023]. See the Terms and Conditions (https://onlinelibrary.wiley.com/terms-and-conditions) on Wiley Online Library for rules of use; OA articles are governed by the applicable Creative Commons License

modified MIRD phantom geometry in our simulations; bone marrow volumes are visible within several bones in this figure.

To calculate the dose to bone marrow in simulation, we tallied the energy deposited to each of our marrow volumes within Geant4 and calculated absorbed dose (*D*) by dividing energy deposited by mass for each marrow volume. We then translated absorbed dose to dose equivalent (*H*) using radiation quality factors (*Q*).[17] The dose equivalent for the collective bone marrow was then calculated by taking the mass-weighted average of dose equivalent over all bone marrow volumes.

To evaluate the impact of our modifications to the MIRD phantom, we compared our bone marrow dosimetry method with three prior methods from the literature. These prior approaches were developed over the past several decades to estimate bone marrow dose indirectly because the MIRD phantom does not define bone marrow volumes. The first method we replicated was that which was presented in the early MIRD documentation.[12] For this method, we assumed a bone and marrow mixture to be uniformly distributed throughout the bone volume, where the density and chemical composition were a weighted composite of bone and marrow. The bone marrow dose was taken as the average skeletal dose to the homogeneous bone/marrow volumes. The second method simply considered the energy deposition in solid bone, although the bone marrow dose was estimated based on the bone marrow distribution.[13] The third method was to calculate and average the soft tissue dose from other organs within the MIRD phantom and assign an average soft tissue dose to the total bone marrow volume.[6]

To explore the impact of modifying the phantom over the range of applications where MIRD phantoms are used, we chose to compare bone marrow dose calculations from our improved fidelity MIRD phantom in medical, occupational, and space-related exposure example scenarios.

For the medical example, we selected posterior-anterior exposure orientation and simulated a standard clinical chest x-ray examination extending from the diaphragm to clavicle (see Figure 2) using a point source collimated to a 35.6 cm × 43.2 cm (14″ × 17″) photon field simulating a 183-cm source-to-image distance and a 5.1-cm patient-to-detector distance. Detector assembly and patient support were not modeled, so backscatter from those were not accounted for. We selected monoenergetic x-rays spanning the relevant clinical energies (20, 30, 40, 50, 60, 80, 100, 120, and 140 keV), as well as typical polychromatic diagnostic x-ray spectra (110, 125, and 140 kVp) derived from a semi-empirical computational method (see Figure 3).[18,19] To compare the polychromatic x-ray spectra and the monoenergetic beams, we converted the spectra to equivalent energy based on their half-value layer and mass attenuation coefficients as described by Johns and Cunningham.[20] For the clinical x-ray spectra used in our medical example, the equivalent energies are provided in Table 2.

For the occupational exposure example, we selected the anterior-posterior (AP) and isotropic orientations from the ICRP reference fields,[21] and simulated exposure to common radioactive isotopes cesium (^{137}Cs) and cobalt (^{60}Co). The AP exposure used a 200 cm × 40 cm planar source 1 m in front of the phantom (see Figure 4). The isotropic exposure used an isotropic photon source around the phantom (see Figure 5) with ^{137}Cs (0.662 MeV) and ^{60}Co (1.173 and 1.332 MeV).

For the space radiation example, we selected an isotropic orientation based on the characteristics of the space radiation environment.[22] We simulated exposure to galactic cosmic ray radiation (see Figure 6). The galactic cosmic ray radiation environment consists of ions from protons to iron, at energies spanning ~MeV to ~TeV.[22] To simulate galactic cosmic ray radiations for the space example, we selected a mixture of ions according to their distribution[22] and monoenergetic

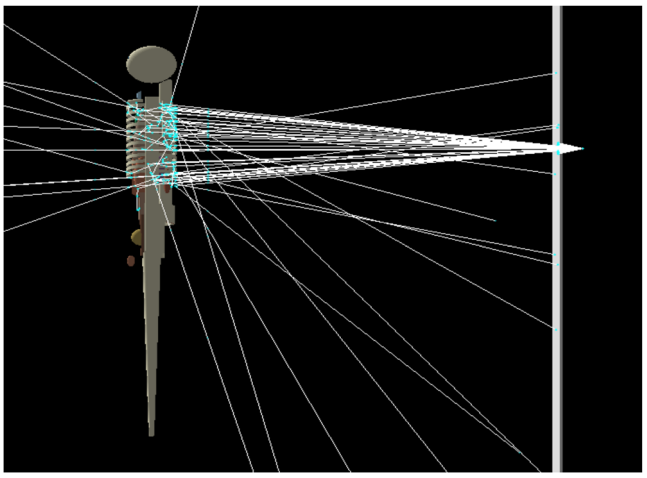

FIGURE 2 Medical internal radiation dose phantom under 125 kVp posterior-anterior diagnostic x-ray irradiation modeled using Geant4 to show geometry.

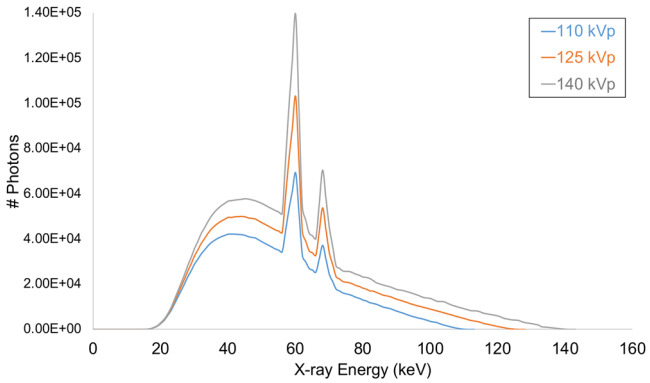

FIGURE 3 X-ray spectra for medical example.

TABLE 2 Equivalent photon energy for clinical diagnostic x-ray spectra.

kVp	hν (keV)
110	40
125	43
140	46

23987324, 2023, 1, Downloaded from https://onlinelibrary.wiley.com/doi/10.1002/pro6.1189 by Rice University, Wiley Online Library on [24/04/2023]. See the Terms and Conditions (https://onlinelibrary.wiley.com/terms-and-conditions) on Wiley Online Library for rules of use; OA articles are governed by the applicable Creative Commons License

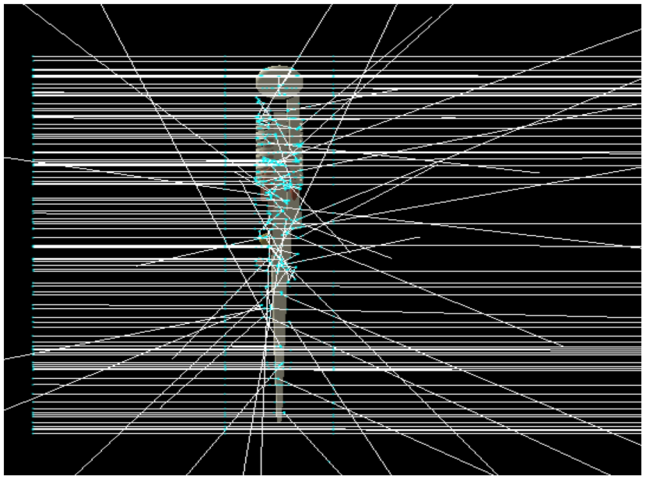

FIGURE 4 Medical internal radiation dose phantom under anterior-posterior gamma irradiation at 0.662 MeV, as modeled using Geant4.

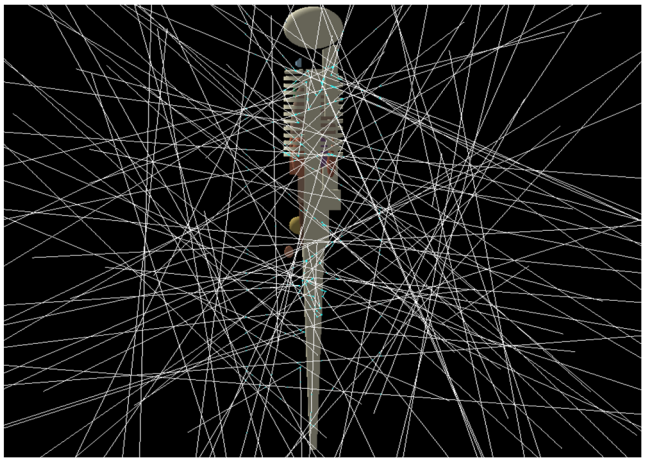

FIGURE 5 Medical internal radiation dose phantom under isotropic gamma irradiation at 0.662 MeV, as modeled using Geant4.

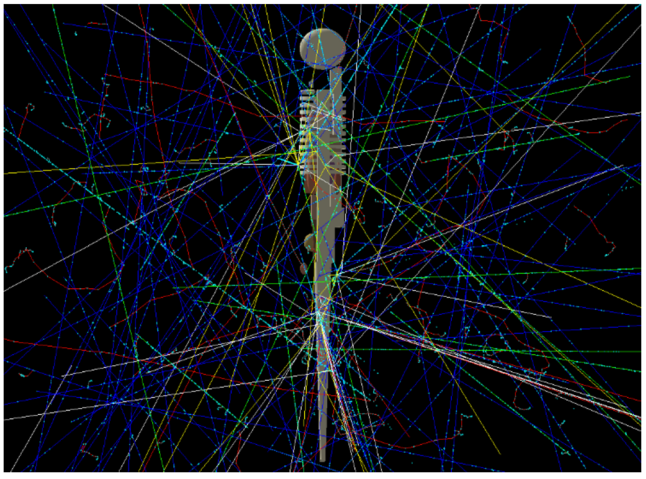

FIGURE 6 Medical internal radiation dose phantom under isotropic galactic cosmic ray irradiation at 1 GeV as modeled using Geant4.

radiation at energies of 10 MeV, 100 MeV, 1 GeV, 10 GeV, 100 GeV, and 1 TeV.

The range of conditions evaluated in the present study is shown in Table 3.

3 | RESULTS

We compared the present dosimetry results using the improved fidelity MIRD phantom with the results from the three bone marrow dose estimation methods (summarized in Table 3). Figures 7–10 show the relative dose equivalent delivered to the bone marrow in each case calculated by each of the three indirect estimation methods, as well as by improved fidelity MIRD calculations.

3.1 | Medical example

For the medical example, we simulated bone marrow dose from both monoenergetic photons and typical clinical diagnostic x-ray spectra sources. Figure 7 shows that the improved fidelity MIRD model reports a smaller bone marrow dose than the traditional methods based on a proportion of solid bone dose or an average homogeneous bone/marrow volume dose. At clinical energies, the dose from the improved fidelity model was lower by a factor of three than the solid bone approach, and lower by a factor of two than the bone/marrow mixture approach. In contrast, the improved fidelity model agreed reasonably well with the average soft-tissue dose. This substantial spread in results highlights the dramatic difference in simulated bone marrow dose between different methods used in the literature.

3.2 | Occupational example

Figures 8 and 9 show the calculated bone marrow dose from the AP and isotropic irradiation cases. No significant difference in bone marrow dose equivalent was found between with the improved fidelity MIRD phantom or any of the three prior estimation methods at gamma energies from common radioactive isotopes in the AP or isotropic orientations. The difference between bone marrow dose values from the three prior estimation methods and those reported from the improved fidelity MIRD model were within the envelope defined by the error bars established as the standard deviation of the improved fidelity MIRD data. Thus, the differences in dose values are not statistically significant, leaving us to conclude that any of the estimation values would yield similar values.

3.3 | Space radiation example

Figure 10 shows that, similar to the occupational example, there is no significant difference in bone marrow dose equivalent, as calculated with the improved fidelity MIRD phantom or any of the three

23987324, 2023, 1, Downloaded from https://onlinelibrary.wiley.com/doi/10.1002/pro6.1189 by Rice University, Wiley Online Library on [24/04/2023]. See the Terms and Conditions (https://onlinelibrary.wiley.com/terms-and-conditions) on Wiley Online Library for rules of use; OA articles are governed by the applicable Creative Commons License

TABLE 3 Scenario definitions for bone marrow dose.

Example type	Radiation field	Radiation species	Energy	Dosimetry method
Medical	PA	X-ray	20, 30, 40, 50, 60, 70, 80, 100, 120, 140 keV	1. Improved fidelity MIRD dose 2. Proportion of bone dose
			110, 125, 140 kVp	3. Proportion of homogeneous bone/marrow dose 4. Average soft tissue dose
Radiation protection	AP iso	Gamma	0.662 MeV 1.17, 1.33 MeV	1. Improved fidelity MIRD dose 2. Proportion of bone dose 3. Proportion of homogeneous bone/marrow dose 4. Average soft tissue dose
Space radiation	Iso	Proton Alpha Heavy ion	10, 100 MeV 1, 10, 100 GeV 1 TeV	1. Improved fidelity MIRD dose 2. Proportion of bone dose 3. Proportion of homogeneous bone/marrow dose 4. Average soft tissue dose

AP, anterior-posterior; iso, isotropic; MIRD, medical internal radiation dose; PA, posterior-anterior.

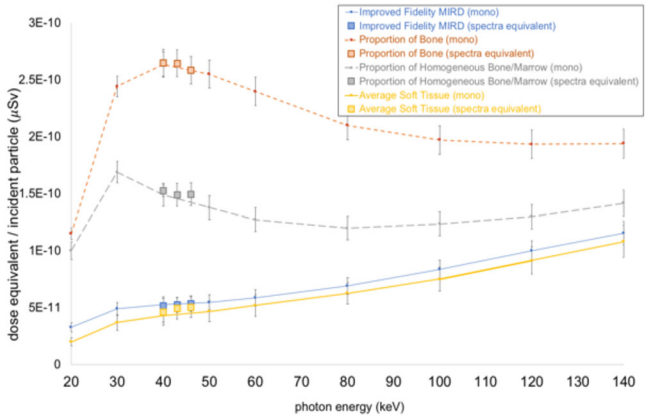

FIGURE 7 Bone marrow dose equivalent in the medical example, as calculated via four different dosimetry methods, using monoenergetic photons and spectral x-ray sources. Error bars represent the standard deviation from Monte Carlo simulations. MIRD, medical internal radiation dose.

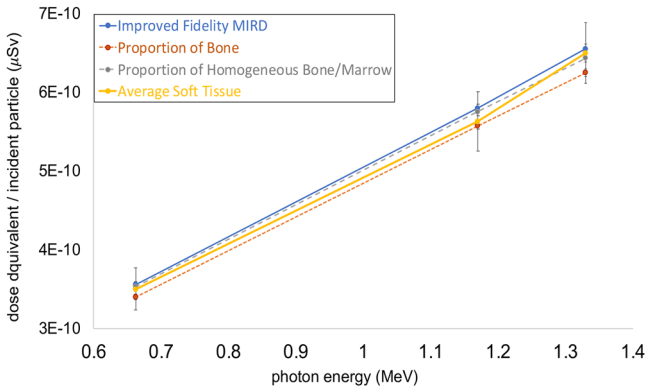

FIGURE 8 Bone marrow dose equivalent for radiation protection (anterior-posterior) example. Error bars represent the standard deviation from the Monte Carlo simulations. MIRD, medical internal radiation dose.

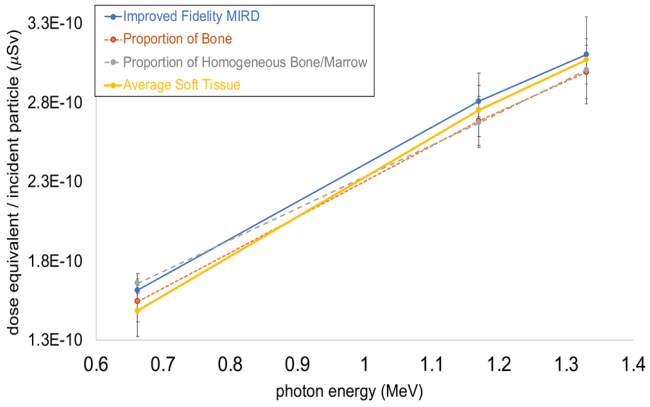

FIGURE 9 Bone marrow dose equivalent for radiation protection (iso) example. Error bars represent the standard deviation from the Monte Carlo simulations. MIRD, medical internal radiation dose.

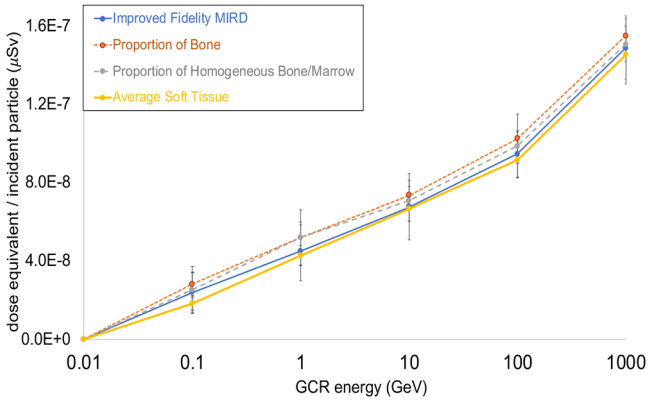

FIGURE 10 Bone marrow dose equivalent for space radiation (iso) example. Galactic cosmic rays (GCRs) included ions from $Z = 1$ to $Z = 26$ at the energies indicated. Error bars represent the standard deviation from the Monte Carlo simulations. MIRD, medical internal radiation dose.

23987324, 2023, 1, Downloaded from https://onlinelibrary.wiley.com/doi/10.1002/pro6.1189 by Rice University, Wiley Online Library on [24/04/2023]. See the Terms and Conditions (https://onlinelibrary.wiley.com/terms-and-conditions) on Wiley Online Library for rules of use; OA articles are governed by the applicable Creative Commons License

prior estimation methods at galactic cosmic ray energies in an isotropic orientation. In this example as well, the difference between bone marrow dose values from the three prior estimation methods and those reported from the improved fidelity MIRD model were within the envelope defined by the error bars established as the standard deviation of the improved fidelity MIRD data. Thus, the differences in dose values are not statistically significant, leaving us to conclude that any of the models of active bone marrow, including the simplest dose estimation method (average soft tissue dose) can be used equivalently for space radiation applications involving isotropic galactic cosmic ray radiation in this energy range.

4 | DISCUSSION

Several bone marrow dose estimation methods were evaluated in the present study across example human exposure scenarios. In specific example cases, the choice of bone marrow dosimetry method affected the estimated bone marrow dose by a substantial degree, whereas in other example cases, the estimated bone marrow dose did not vary significantly based on the choice of dosimetry method.

The bone marrow dose differences observed in the medical example are consistent with the higher atomic number (Z) of the solid bone and homogeneous bone/marrow volumes. At these photon energies, photon interactions are dominated by the photoelectric effect, which depends on the target material atomic number by approximately Z^3. Due to this effect, the total mass attenuation coefficient (μ/ρ) at clinical diagnostic x-ray energies varies by approximately a factor of three between soft tissue and bone.[20] This is consistent with the difference in bone marrow dose between the solid bone and improved fidelity approaches. Similarly, the uniform mixture of bone and marrow would be expected to over-respond compared with soft tissue by approximately a factor of two, which is similar to the differences seen in Figure 7. The simple soft tissue average dose for the medical example is closest to what we calculated with the improved fidelity MIRD model, although this method underestimates the bone marrow dose by between 6% at 140 keV and 30% at 20 keV. This discrepancy is consistent with the presence of buildup in the bone tissue, which creates an increase in bone marrow dose near the interface with solid bone.[23]

In the occupational and space radiation examples, higher-energy photons and particles are involved. These high-energy photons interact through Compton scattering, which is a process independent of atomic number. Similarly, for high-energy charged particles, mass stopping power ratios do not change dramatically with atomic number. Because of the insensitivity of dose to atomic number at these high photon or charged particle energies, actual material composition has minimal impact. Therefore, the estimated bone marrow dose is substantially independent of the method by which the bone marrow is estimated for these exposure scenarios.

In addition to dosimetric considerations, a higher fidelity model has benefits over indirect estimation. It is more robust for a broad-spectrum, because low energy photons exhibit major differences in interactions. Furthermore, our improved fidelity MIRD model is suitable for any study where estimation of dose to a specific volume of marrow is required.

These results indicate that prior indirect estimation methods using the MIRD phantom can potentially overestimate the active bone marrow dose by more than a factor of three across clinical diagnostic x-ray energies, confirming limitations provided in the MIRD literature.[2–4] Because active bone marrow dose is assigned a high tissue weighting factor in the calculation of effective dose,[17] and in translation to the risk of radiation-induced cancer incidence and mortality, a discrepancy of this size could create a sizeable overestimate of the risk of radiation-induced cancer for a given exposure. Although our improved fidelity model is still not an exact replica of the human body, the bone marrow representation and direct dose tallying could improve the accuracy of effective dose and the estimated risk of radiation-induced cancers.

5 | CONCLUSIONS

In summary, our improved fidelity MIRD phantom includes direct calculation of bone marrow dose equivalents and increases the realism of the stylized phantom. Comparing direct calculations of bone marrow dose using the higher fidelity MIRD phantom to indirect dose calculations via prior methods across several examples from medical, occupational, and space radiation applications shows that there are differences in the estimated dose to bone marrow that are most pronounced in low-energy applications (<200 keV). Differences in this diagnostic energy range can exceed a factor of three. In applications such as these, the method of evaluating dose to bone marrow is very important and should be implemented with due consideration. Particularly, in medical applications involving lower-energy x-rays, it is recommended that an improved fidelity MIRD phantom be used, which can improve the accuracy of dose calculation to bone marrow.

ACKNOWLEDGMENTS

This work was partially funded by the first author's graduate fellowship provided by The Aerospace Corporation, El Segundo, California.

CONFLICT OF INTEREST STATEMENT

The authors declare no conflicts of interest.

REFERENCES

1. Peterson L, Kovyrshina T. Adjustment of lifetime risks of space radiation-induced cancer by the healthy worker effect and cancer misclassification. *Heliyon*. 2015:e00048.
2. Carlsen T, Peterson L, Ulsh B, Werner C, Purvis K, Sharber A. Radionuclide contamination at Kazakhstan's Semipalatinsk test site: implications on human and ecological health. *Hum Ecol Risk Assess*. 2001;7(4):943-955.
3. Peterson L, Miller R. Association between radioactive fallout from 1951–1962 US nuclear tests at the Nevada test site and cancer mortality in midwestern US populations. *Russian J Ecol*. 2008;39(7):495-509.
4. National Research Council. *Effects of Ionizing Radiation: Atomic Bomb Survivors and Their Children (1945-1995)*, (1998).

23987324, 2023, 1, Downloaded from https://onlinelibrary.wiley.com/doi/10.1002/pro6.1189 by Rice University, Wiley Online Library on [24/04/2023]. See the Terms and Conditions (https://onlinelibrary.wiley.com/terms-and-conditions) on Wiley Online Library for rules of use; OA articles are governed by the applicable Creative Commons License

5. Snyder W, Ford M, Warner G. *A Tabulation of Dose Equivalent Per Microcurie-Day for Source and Target Organs of an Adult for Various Radionuclides*. Oak Ridge National Laboratory; 1974. Report No. ORNL-5000.
6. Cristy M, Eckerman K. *Specific Absorbed Fractions of Energy at Various Ages From Internal Photon Sources – VII Adult Male*. Oak Ridge National Laboratory; 1987. Report No. ORNL/TM-8381/V7.
7. Cristy M, Eckerman K. *Specific Absorbed Fractions of Energy at Various Ages From Internal Photon Sources – I Methods*. Oak Ridge National Laboratory; 1987. Report No. ORNL/TM-8381/V1.
8. Dant J, Richardson R, Nie L. Monte Carlo simulation of age-dependent radiation dose from alpha- and beta-emitting radionuclides to critical trabecular bone and bone marrow targets. *Phys Med Biol*. 2013;58:3301-3319.
9. Gialousis G, Yakoumakis E, Dimitriadis A, et al. Monte Carlo estimation of radiation doses in red bone marrow and breast in common pediatric x-ray examinations. *Health Phys*. 2008;95(3):331-336.
10. Kvinnsland Y, Skretting A, Bruland Ø. Radionuclide therapy with bone-seeking compounds: Monte Carlo calculations of dose-volume histograms for bone marrow in trabecular bone. *Phys Med Biol*. 2001;46:1149-1161.
11. Nie H, Richardson R. Radiation dose to trabecular bone marrow stem cells from 3H, 14C, and selected α-emitters incorporated in a bone remodeling compartment. *Phys Med Biol*. 2009;54:963-979.
12. Snyder W, Ford M, Warner G. Estimates of specific absorbed fractions for photon sources uniformly distributed in various organs of a heterogeneous phantom. *Medical Internal Radiation Dose (MIRD) Pamphlet*. 1978(5).
13. Xu W, Eckerman K. *Handbook of Anatomical Models for Radiation Dosimetry*. CRC Press; 2010.
14. Agostinelli S, Allison J, Amako K, et al. GEANT4: a simulation toolkit. *Nucl Phys A*. 2003;506(3):250-303.
15. Cristy M. Active bone marrow distribution as a function of age in humans. *Phys Med Biol*. 1981;26(3):389-400.
16. Martins M, Sivla R, Begalli M, Queiroz Filho P, Souza-Santos D, Pia M. *Anthropomorphic phantoms and GEANT4-based implementations for dose calculation*. Proceedings of the 2009 IEEE Nuclear Science Symposium; 2009. 25–31 October 2009.
17. International Commission on Radiological Protection. *The 2007 Recommendations of the International Commission on Radiological Protection*. ICRP Publication 103; 2007.
18. Boone J, Chavez A. Comparison of x-ray cross sections for diagnostic and therapeutic medical physics. *Med Phys*. 1996;23(12):1997-2005.
19. Boone J, Siebert JA. An accurate method for computer-generating tungsten anode x-ray spectra from 30 to 140 kV. *Med Phys*. 1997;24(11):1661-1670.
20. Johns H, Cunningham J. *The Physics of Radiology*. 4th ed. Charles River Media; 1983.
21. International Commission on Radiological Protection. *Compendium of Dose Coefficients Based on ICRP Publication 60*. ICRP Publication 119; 2012.
22. Cucinotta F, Kim M, Chappell L. *Space Radiation Cancer Risk Projections and Uncertainties –2012*. National Aeronautics and Space Administration; 2013. Report No. NASA-TP-2013-217375.
23. Hendee W, Ritenour ER. *Medical Imaging Physics*, 4th ed. Wiley-LISS; 2002.

How to cite this article: Ferrone KL, Willis CE, Guan F, Ma J, Peterson LE, Kry SF. Evaluating bone marrow dosimetry with the addition of bone marrow structures to the medical internal radiation dose phantom. *Prec Radiat Oncol*. 2023;7:27–35. https://doi.org/10.1002/pro6.1189

23987324, 2023, 1, Downloaded from https://onlinelibrary.wiley.com/doi/10.1002/pro6.1189 by Rice University, Wiley Online Library on [24/04/2023]. See the Terms and Conditions (https://onlinelibrary.wiley.com/terms-and-conditions) on Wiley Online Library for rules of use; OA articles are governed by the applicable Creative Commons License

APPENDIX 1

Bone	Mass (g)	Net volume (cm^3)	Density (g/cm^3)	% Total active marrow	Marrow volume shape	Marrow volume calculation	Marrow G4 volume dimensions (cm)
Cranium	1398.05	728.15	1.92	–	–	–	–
Cranium marrow	126.00	118.87	1.06	8.40%	Subtraction ellipsoid	$V = 4/3\pi$ (ABC-abc)	$A = 6.48, B = 9.48, C = 7.48$ $a = 6.32, b = 9.32, c = 7.32$
Left scapula	155.77	81.13	1.92	–	–	–	–
Left scapula marrow	21.00	19.81	1.06	1.40%	Subtraction elliptical tube segment	$V = \pi$ (ABH-abh) $\times \theta/2\pi$	$A = 18.2, B = 9.8, H = 8.199$ $a = 17.8, b = 9.8, h = 8.199$ $\theta \sim 0.4$ rad
Right scapula	156.25	81.38	1.92	–	–	–	–
Right scapula marrow	21.00	19.81	1.06	1.40%	Subtraction elliptical tube segment	$V = \pi$ (ABH-abh) $\times \theta/2\pi$	$A = 18.2, B = 9.8, H = 8.199$ $a = 17.8, b = 9.8, h = 8.199$ $\theta \sim 0.4$ rad
Left clavicle	15.38	8.01	1.92	–	–	–	–
Left clavicle marrow	6.00	5.66	1.06	0.40%	Torus segment	$V = \pi r^2 \times 2\pi R \times \theta/2\pi$	$r = 0.5, R = 10, \theta = 0.69$ rad
Right clavicle	15.38	8.01	1.92	–	–	–	–
Right clavicle marrow	6.00	5.66	1.06	0.40%	Torus segment	$V = \pi r^2 \times 2\pi R \times \theta/2\pi$	$r = 0.5, R = 10, \theta = 0.69$ rad
Rib 1	66.62	34.70	1.92	–	–	–	–
Rib 1 marrow	24.00	22.64	1.06	1.60%	Subtraction elliptical tube	$V = \pi$ (ABH-abh)	$A = 16.85, B = 9.65,$ $H = 1.398$ $a = 16.65, b = 9.45, h = 1.398$
Rib 2	67.52	35.17	1.92	–	–	–	–
Rib 2 marrow	24.00	22.64	1.06	1.60%	Subtraction elliptical tube	$V = \pi$ (ABH-abh)	$A = 16.85, B = 9.65,$ $H = 1.398$ $a = 16.65, b = 9.45, h = 1.398$
Rib 3	68.35	35.60	1.92	–	–	–	–
Rib 3 marrow	24.00	22.64	1.06	1.60%	Subtraction elliptical tube	$V = \pi$(ABH-abh)	$A = 16.85, B = 9.65,$ $H = 1.398$ $a = 16.65, b = 9.45, h = 1.398$
Rib 4	67.37	35.09	1.92	–	–	–	–
Rib 4 marrow	24.00	22.64	1.06	1.60%	Subtraction elliptical tube	$V = \pi$ (ABH-abh)	$A = 16.85, B = 9.65,$ $H = 1.398$ $a = 16.65, b = 9.45, h = 1.398$
Rib 5	67.43	35.12	1.92	–	–	–	–
Rib 5 marrow	24.00	22.64	1.06	1.60%	Subtraction elliptical tube	$V = \pi$ (ABH-abh)	$A = 16.85, B = 9.65,$ $H = 1.398$ $a = 16.65, b = 9.45, h = 1.398$
Rib 6	67.22	35.01	1.92	–	–	–	–
Rib 6 marrow	24.00	22.64	1.06	1.60%	Subtraction elliptical tube	$V = \pi$(ABH-abh)	$A = 16.85, B = 9.65,$ $H = 1.398$ $a = 16.65, b = 9.45, h = 1.398$
Rib 7	67.54	35.18	1.92	–	–	–	–
Rib 7 marrow	24.00	22.64	1.06	1.60%	Subtraction elliptical tube	$V = \pi$ (ABH-abh)	$A = 16.85, B = 9.65,$ $H = 1.398$ $a = 16.65, b = 9.45, h = 1.398$

(Continued)

23987324, 2023, 1, Downloaded from https://onlinelibrary.wiley.com/doi/10.1002/pro6.1189 by Rice University, Wiley Online Library on [24/04/2023]. See the Terms and Conditions (https://onlinelibrary.wiley.com/terms-and-conditions) on Wiley Online Library for rules of use; OA articles are governed by the applicable Creative Commons License

Bone	Mass (g)	Net volume (cm^3)	Density (g/cm^3)	% Total active marrow	Marrow volume shape	Marrow volume calculation	Marrow G4 volume dimensions (cm)
Rib 8	67.43	35.12	1.92	–	–	–	–
Rib 8 marrow	24.00	22.64	1.06	1.60%	Subtraction elliptical tube	$V = \pi$ (ABH-abh)	$A = 16.85, B = 9.65, H = 1.398$ $a = 16.65, b = 9.45, h = 1.398$
Rib 9	67.91	35.37	1.92	–	–	–	–
Rib 9 marrow	24.00	22.64	1.06	1.60%	Subtraction elliptical tube	$V = \pi$ (ABH-abh)	$A = 16.85, B = 9.65, H = 1.398$ $a = 16.65, b = 9.45, h = 1.398$
Rib 10	67.14	34.97	1.92	–	–	–	–
Rib 10 marrow	24.00	22.64	1.06	1.60%	Subtraction elliptical tube	$V = \pi$ (ABH-abh)	$A = 16.85, B = 9.65, H = 1.398$ $a = 16.65, b = 9.45, h = 1.398$
Rib 11	67.10	34.95	1.92	–	–	–	–
Rib 11 marrow	24.00	22.64	1.06	1.60%	Subtraction elliptical tube	$V = \pi$ (ABH-abh)	$A = 16.85, B = 9.65, H = 1.398$ $a = 16.65, b = 9.45, h = 1.398$
Rib 12	67.95	35.39	1.92	–	–	–	–
Rib 12 marrow	24.00	22.64	1.06	1.60%	Subtraction elliptical tube	$V = \pi$ (ABH-abh)	$A = 16.85, B = 9.65, H = 1.398$ $a = 16.65, b = 9.45, h = 1.398$
Upper spine	136.73	71.21	1.92	–	–	–	–
Upper spine marrow	58.50	55.19	1.06	3.90%	Elliptical tube	$V = \pi$ (abh)	$a = 1.53, b = 1.91, h = 6$
Middle lower spine	407.17	212.07	1.92	–	–	–	–
Middle lower spine marrow	574.50	541.98	1.06	38.30%	Elliptical tube	$V = \pi$ (abh)	$a = 1.7, b = 2.12, h = 47.98$
Pelvis	681.71	355.06	1.92	–	–	–	–
Pelvis marrow	262.50	247.64	1.06	17.50%	Subtraction elliptical tube segment	$V = \pi$ (ABH-abh) ˜× $\theta/2\pi$	$A = 11.68, B = 11.79, H = 21.998$ $a = 11.51, b = 11.51, h = 21.998$ $\theta \sim \pi$ rad
Left leg bone	2596.48	1352.33	1.92	–	–	–	–
Left leg bone marrow	50.25	47.41	1.06	3.35%	Cylinder	$V = \pi r^2$ h	$r = 0.434, h = 79.798$
Right leg bone	2596.48	1352.33	1.92	–	–	–	–
Right leg bone marrow	50.25	47.41	1.06	3.35%	Cylinder	$V = \pi r^2$ h	$r = 0.434, h = 79.798$
Left arm bone	1541.62	802.93	1.92				
Left arm bone marrow	17.25	16.27	1.06	1.15%	Elliptical tube	$V = \pi$ (abh)	$a = 0.197, b = 0.38, h = 69$
Right arm bone	1539.85	802.01	1.92				
Right arm bone marrow	17.25	16.27	1.06	1.15%	Elliptical tube	$V = \pi$ (abh)	$a = 0.197, b = 0.38, h = 69$
Total bone mass	12050.44						
Total active marrow mass	1498.50						

23987324, 2023, 1, Downloaded from https://onlinelibrary.wiley.com/doi/10.1002/pro6.1189 by Rice University, Wiley Online Library on [24/04/2023]. See the Terms and Conditions (https://onlinelibrary.wiley.com/terms-and-conditions) on Wiley Online Library for rules of use; OA articles are governed by the applicable Creative Commons License